Journal of Controlled Release 163 (2012) 249–255

Contents lists available at SciVerse ScienceDirect

Journal of Controlled Release

journal homepage: www.elsevier.com/locate/jconrel

NANOMEDICINE

In vivo NIRF and MR dual-modality imaging using glycol chitosan nanoparticles

Jaehong Key [a,b,c], Christy Cooper [b,c,d], Ah Young Kim [e], Deepika Dhawan [d], Deborah W. Knapp [d], Kwangmeyung Kim [e], Jae Hyung Park [f], Kuiwon Choi [e], Ick Chan Kwon [e], Kinam Park [a,g], James F. Leary [a,b,c,d,*]

[a] Weldon School of Biomedical Engineering, Purdue University, West Lafayette, IN 47906, United States
[b] Birck Nanotechnology Center at Discovery Park, Purdue University, West Lafayette, IN 47906, United States
[c] Bindley Bioscience Center at Discovery Park, Purdue University, West Lafayette, IN 47906, United States
[d] School of Veterinary Medicine, Department of Basic Medical Sciences, Purdue University, West Lafayette, IN 47906, United States
[e] Center for Theragnosis, Biomedical Research Institute, Korea Institute of Science and Technology (KIST), 39-1 Hawolgok-dong, Seongbuk-gu, Seoul 136–791, Republic of Korea
[f] Department of Polymer Science and Engineering, Sungkyunkwan University, Suwon, Gyeonggi 440-746, Republic of Korea
[g] Department of Pharmaceutics, Purdue University, West Lafayette, IN 47907, United States

ARTICLE INFO

Article history:
Received 6 April 2012
Accepted 28 July 2012
Available online 11 August 2012

Keywords:
Cancer
MRI
NIRF imaging
Chitosan nanoparticle
Dual-modality imaging

ABSTRACT

One difficulty of diagnosing and treating cancer is that it is very challenging to detect cancers in the early stages before metastasis occurs. A variety of imaging modalities needs to be used from non-invasive, moderate resolution modalities, such as magnetic resonance imaging (MRI) to very high-resolution (e.g. fluorescence) imaging that can help guide surgeons during a surgical operation. While MRI can have relatively high resolution and deep penetration to visualize soft tissues, low sensitivity of MRI frequently requires tumor imaging agents to enhance the MRI contrast at the tumor site. At the other end of the resolution spectrum, near infrared fluorescence (NIRF) imaging has very high sensitivity but frequently cannot be utilized for initial human in vivo imaging due to its very limited penetration depth. To combine the advantages of each imaging modality we have constructed MRI and NIRF dual-modality nanoparticles using glycol chitosan, Cy5.5, and superparamagnetic iron oxide nanoparticles (SPIOs). We have demonstrated these advantages for dual-modality, in vivo tumor imaging in mice. Our studies suggest the potential use of NIRF and MR dual modality imaging for human cancer diagnosis.

1. Introduction

Cancer is one of the most challenging medical conditions to treat. Cancer affects various organs and can occur in nearly every tissue in the body [1]. One difficult aspect of treating cancer is to find it at the early stages before the cancer metastasizes through the lymph systems and blood vessels. In addition, early detection is closely correlated to the survival rate for most cancers. For example, the early detection of cancers including breast, colorectal, and prostate led to approximately 80% survival rate for 10 years [2,3]. That is, the early detection of cancer is one of the critical factors to treat cancer. To find tumor in the human body, we are using imaging modalities such as X-ray, computed tomography (CT), positron emission tomography (PET), ultrasound (US), magnetic resonance imaging (MRI), and so on. However, current imaging modalities cannot readily discover early stage cancers in the human body due to either limited spatial resolution or to the low sensitivity of imaging agents.

Optical imaging techniques of particular interest have made it possible to understand the characteristics of cancer such as the enhanced permeability and retention (EPR) effect and to demonstrate various ways to effectively visualize cancer through in vivo systems as well as in vitro [4]. Near infrared fluorescence (NIRF) can specially penetrate a couple of centimeters in tissues because it is minimally absorbed by hemoglobin and water in the body, so it can be applied to in vivo systems [5]. The NIRF dyes can be used at nano-molar to pico-molar concentrations [6]. For instance, our previous studies of hydrophobically modified glycol chitosan (HGC) nanoparticles demonstrated excellent capabilities in optical imaging to visualize early stage tumor and to deliver anti-cancer drugs in mice [7,8]. However, the penetration depth in optical imaging is still very limited, so NIRF dyes cannot be directly visualized inside large animals such as dogs and pigs, as well as in humans. On the other hand, magnetic resonance imaging (MRI) is one of the most powerful imaging modalities for high resolution human body images. Currently, MRI is being developed to provide better anatomical, physiological, and even molecular information [9]. However, the current limitation of MRI is the low sensitivity of imaging agents. While the low sensitivity can be improved either by the development of new MR contrast agents with higher sensitivity or MR machines with higher magnetic fields, the

* Corresponding author at: Birck Nanotechnology Center at Discovery Park, Purdue University, West Lafayette, IN 47906, United States.
E-mail address: jfleary@purdue.edu (J.F. Leary).

0168-3659/$ – see front matter © 2012 Elsevier B.V. All rights reserved.
http://dx.doi.org/10.1016/j.jconrel.2012.07.038

current MRI techniques are inferior to the sensitivity of optical imaging. Thus, we reported the NIRF and MR dual-modality nanoparticles using glycol chitosan nanoparticles, gadolinium, and NIRF dyes as an alternative in which gadolinium also worked as an effective positive MR contrast agent [10]. However, gadolinium based contrast agents have a limitation in that these agents have triggered the development of nephrogenic systemic fibrosis (NSF) which is a fibrosing disorder that arises in patients with renal impairment. As a result, the U.S. Food and Drug Administration (FDA) and the European Medicines Agency (EMEA) have announced safety alerts and recommendations to the uses for patients with renal impairment [11].

Due to the drawbacks of gadolinium, several trials using SPIOs and fluorophores had been done by different groups [12]. SPIOs have relatively low toxicity and they were also characterized to have excellent negative MR contrast effects and hyperthermia effects by converting the energy absorbed from an AC magnetic field to the thermal energy [13]. However, these trials must be improved in terms of sensitivity, specificity, and/or low toxicity for successful cancer imaging. Successful cancer imaging is mainly affected by various physicochemical properties of NPs such as size, shape, and zeta-potentials. Therefore, one of the most important factors for the cancer imaging is to choose a good carrier to deliver MR contrast agents and optical probes at the tumor site. From this point of view, the combination of glycol chitosan modified NPs with 5β cholanic acid (HGC) and SPIOs can be a promising way for optical and MR dual-modality cancer imaging because low toxicity HGC NPs have displayed excellent tumor imaging ability in optical imaging, allowing them to circulate for a long time in the blood stream [14]. In addition, the HGC NPs are good carriers to deliver anti-cancer drugs such as paclitaxel and camptothecin [15]. In this paper, HGC NPs were evaluated to deliver SPIOs to the tumor sites. We synthesized the self-assembled glycol chitosan nanoparticles by chemically conjugating it to hydrophobic 5β-cholanic acid and the glycol chitosan (GC) nanoparticles were labeled with near infrared fluorescent dye Cy5.5. Finally, SPIOs were physically encapsulated into the glycol chitosan nanoparticles (Fig. 1A). Among many ways to enhance the T2 contrast effect of SPIOs, the encapsulation of SPIOs in a stable carrier in the blood stream can additionally increase the T2 contrast effects [16]. The encapsulation of SPIOs into the HGC nanoparticle as carriers can have another advantage to improve the T2 contrast effects to the tumor sites.

2. Materials and methods

2.1. Synthesis of glycol chitosan nanoparticles for NIRF and MR dual-modality imaging

Water-soluble glycol chitosan was conjugated to hydrophobic 5β-cholanic acid to form self-assembled nanoparticles in aqueous solution. Glycol chitosan (GC, Mw = 250 kDa, degree of deacetylation = 82.7%), 5β-cholanic acid, 1-ethyl-3-(3-dimethylamniopropyl)-carbodiimide hydrochloride (EDC), and *N*-hydroxysuccinimide (NHS) were purchased from Sigma-Aldrich Corp (St. Louis, MO). The chemicals were purchased as reagent grade and used without further purification. Anhydrous grade methanol and dimethyl sulfoxide (DMSO) were used as solvents. Partial modification of GC for self-assembled nanoparticles was mostly carried out following the earlier study [8]. Briefly, GC (250 mg) was dissolved in distilled water (32 ml). When GC was dissolved completely, EDC (60 mg) was added and followed by methanol (32 ml). In another beaker, 5β-cholanic acid (75 mg) and NHS (36 mg) were dissolved in methanol (64 ml), which was added slowly to the solution of GC with stirring. This mixture was allowed to conjugate for 20 h at room temperature. The solution was dialyzed (MWCO = 10 kDa) to remove un-reacted chemicals and to replace methanol with distilled water. The dialysis was performed by three steps (1:3 (v/v) water/methanol for 1 day; 1:1 (v/v) water/methanol for 1 day, pure water for 2 days). The final GC conjugated with 5β-cholanic acid (23 mol% of amine in GC polymer, feed ratio per monosaccharide) solution in water was lyophilized for 3–4 days and stored at −20 °C. The hydrophobically modified GC conjugates were labeled with NIRF dye, Cy5.5 for NIRF imaging. The mono-reactive N-hydroxysuccinimide ester of cyanine 5.5 (Cy5.5-NHS) was purchased from GE Healthcare Corp (Piscataway, NJ). *N*-Hydroxysuccinimide ester of Cy5.5 was chemically coupled to the GC conjugate (4:1 mole ratio Cy5.5-NHS:GC conjugate). The reaction for GC-Cy5.5coupling was performed in DMSO by slowly dropping Cy5.5 solution in the GC solution while stirring. The mixture was stirred overnight and protected from light. The solution was dialyzed (MWCO = 10 kDa) to remove unreacted Cy5.5 and to replace DMSO with distilled water. Dialysis was performed for 1 day with sodium chloride (100 mM) to enhance the removal of unreacted Cy5.5. Dialysis was additionally performed for 2 days in distilled water without sodium chloride. The final solution was lyophilized for three to four days and stored at −20 °C. Herein hydrophobically modified GC-Cy5.5 nanoparticles are termed as HGC (Fig. 1B).

2.2. Synthesis and loading of superparamagnetic iron oxide nanoparticles

We synthesized monodisperse SPIOs by following the method of Yu et al. [17]. Briefly, we obtained iron oxide hydroxide (FeO(OH)), oleic acid, and 1-octadecene from Sigma-Aldrich (St. Louis, MO). Chloroform and acetone were purchased from Mallinckrodt Baker (Phillipsburg, NJ). All solvents and reagents were used without further purification. A mixture of finely ground FeO(OH) (0.178 g, 2.00 mmol), oleic acid (2.26 g, 8.00 mmol), and 1-octadecene (5.00 g) was heated to 320 °C under stirring and kept at this temperature for 30 min using a heating mantle and temperature controller. This reaction was done under nitrogen atmosphere. This solution was allowed to reflux and subsequently cooled to room temperature. This final solution was a clear black color and the reaction yielded oleic acid-capped iron oxide nanocrystals. Excess oleic acid and unreacted FeO(OH) were eliminated by extracting the nanoparticle suspension using 1:1 (v/v) methanol:chloroform solution. Acetone was then used to precipitate the nanoparticles from octadecene. Once SPIOs were precipitated, the SPIOs were easily isolated using a magnet and then stored in chloroform. The SPIOs were physically loaded into HGC nanoparticles. HGC nanoparticles (12 mg) were dissolved in distilled water (12 ml) using a bath-type sonicator (Bransonic® ultrasonic cleaner, Danbury, CT) for 10 min and by using a probe-type sonicator (Sonics® Vibra-Cell™, Newtown, CT) for 2 min, keeping the temperature at 4 °C with ice water. SPIOs in chloroform were further purified by ethanol as follows. SPIOs (300 μl) and ethanol (1 ml) were mixed by vortexing. The mixture was centrifuged at 10,000 rpm for 7 min. The supernatant was removed. The precipitated SPIOs were re-dispersed in chloroform. The purified SPIOs (18 μl) in chloroform were added to the HGC nanoparticle solution that was prepared in advance. SPIOs were physically loaded into HGC nanoparticles by using a probe-type sonicator for 10 min, keeping the temperature at 4 °C with ice. The final solution was lyophilized for three days and stored at −20 °C under light protection. The SPIOs loaded in HGC nanoparticles were termed here as GS nanoparticles (Fig. 1A).

2.3. Characterizations of GS nanoparticles

TEM images were acquired using a FEI/Philips CM-100 (FEI Company, Hillsboro, OR). Sample preparation was performed as follows. For TEM images, bare SPIOs were diluted in chloroform and GS nanoparticles were diluted in distilled water. The diluted suspensions were sonicated briefly and deposited onto holey carbon TEM grids. After the nanoparticles were dried onto the grids, TEM images were acquired. Also, the hydrodynamic diameter of GS nanoparticles in distilled water was determined at 25 °C by dynamic light scattering, DLS (DynaPro99, Wyatt Technology Corp., Santa Barbara, CA) (Fig. 2C). The data was analyzed using Dynamics v5.26.60 software (Wyatt Technology Corp.). Prior to the DLS measurement, GS nanoparticles were sonicated for 10 min by a bath-type sonicator and for 2 min by a probe-type sonicator, maintaining the suspension temperature at 4 °C

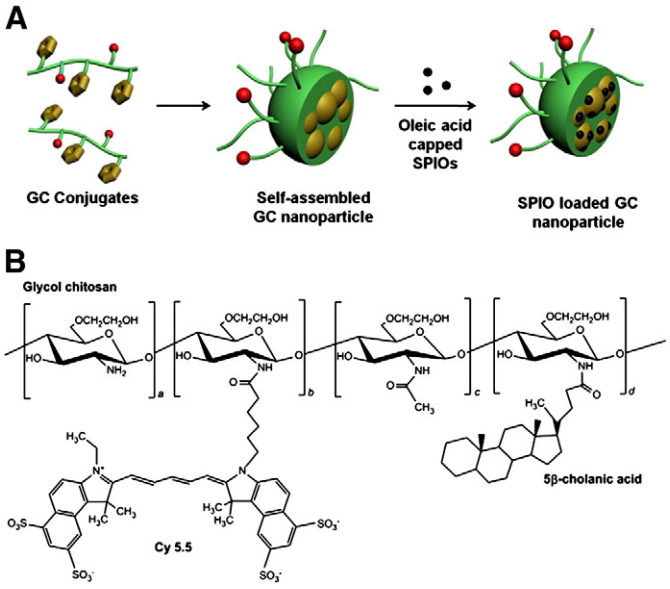

Fig. 1. (A) Schematic diagram of SPIO-loaded glycol chitosan nanoparticles. (B) Chemical structures of glycol chitosan conjugate with hydrophobic 5β-cholanic acid.

on ice. The GS nanoparticles were passed through a syringe filter of pore size 0.8 μm (Millipore™, Billerica, MA). This filtered suspension was used for DLS measurement. Inductively coupled plasma mass spectrometry (ICP-MS) analysis was performed to measure the actual amount of Fe ions in GS nanoparticles. For that, GS nanoparticles (1 mg) were digested respectively by HCl (1 ml) overnight. The digested GS nanoparticles in HCl were heated and evaporated until all the solvent has been evaporated, which were then re-suspended in 2% nitric acid and then filtered by the 0.22 μm syringe filter. The 2% nitric acid solvent was prepared from 75% nitric acid (BDH ARISTAR®, West Chester, PA). The final digested nanoparticles were further diluted to compare with a standard curve of Fe solutions (0, 10, 20, 30, and 40 ppb). The 10 ppb Fe standard solutions were prepared by serial dilutions of 1000 ppm iron

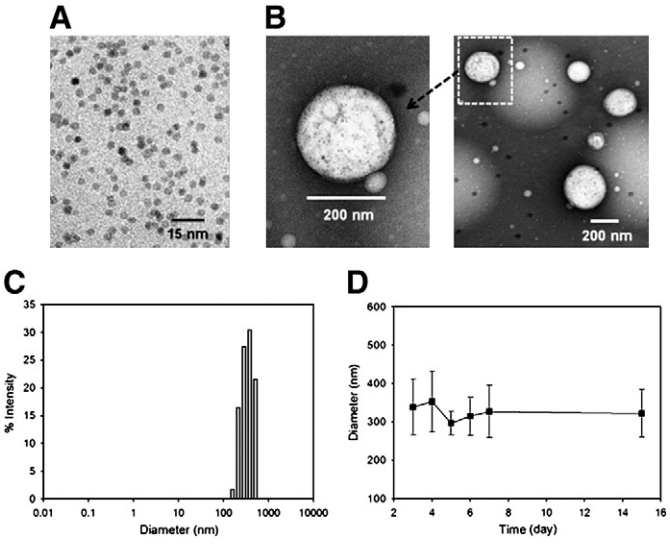

Fig. 2. (A) A TEM image of SPIOs in chloroform. (B) A TEM image of GS nanoparticles in distilled water. The dashed, white rectangle indicates the regions featured in the expanded images. Dashed, black lines and black arrow indicate the expanded region. A white sphere was a GS nanoparticle including many SPIOs. (C) Hydrodynamic diameters of GS nanoparticles measured by dynamic light scattering over time in PBS at 37 °C. (D) Stability test of GS nanoparticles in DLS.

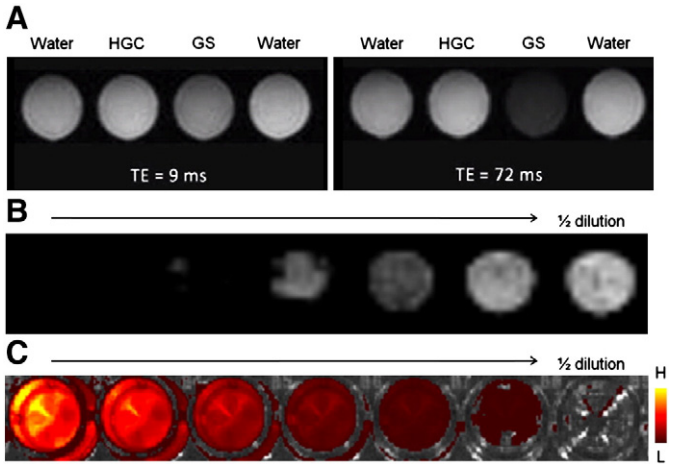

Fig. 3. (A) GS nanoparticles and HGC nanoparticles were compared in terms of T2 MRI contrast effect. At 72 ms of echo time, GS nanoparticles represented the negative contrast effect. (B) The phantom test of GS nanoparticles in MRI. The amount of GS nanoparticles was successively half diluted from left to right. The negative contrast effect by GS nanoparticles was measured in each well. (C) The phantom test of GS nanoparticles in NIRF imaging. The same phantom used in MRI was tested in NIRF imaging, showing NIRF intensities in each well.

ICP-MS standard (Exaxol Corporation, Clearwater, FL) (Supplementary data).

2.4. Evaluation of GS nanoparticles for NIRF and MR dual-modality imaging

The T2 contrast effects of GS nanoparticles and HGC nanoparticles were compared. GS and HGC nanoparticles were dissolved in water and placed into a tissue culture well-plate. MR images were acquired by using a 3 Tesla (T) MR machine (Signa® EXCITE 3.0 T HD system, GE Healthcare, Waukesha, WI), by applying these conditions: T_2-map, coronal plane, 2D, TR = 1500 ms, TE = 9, 17, 26, 35, 44, 53, 62, and 72 ms, FOV = 160 mm, 8HRBRAIN coil, Frequency/Phase = 256/256. For the phantom test of nanoparticles, agarose was purchased from Sigma-Aldrich Corp (St. Louis, MO). 1% (w/v) agarose solution was prepared by boiling a mixture of agarose in distilled water using microwave heating for 45 s. The resulting agarose solution was left on the bench to cool for 5 min, and then 100 μl of GS nanoparticles dissolved in water (1 mg/ml) was added to 1 ml of the agarose. This mixture was poured in the well-plate which solidified at room temperature. MRI for the phantom images was obtained by spin echo, TR = 1500 ms, TE = 100 ms, Frequency/Phase = 256/256, FOV = 100 mm, and 8HRBRAIN coil. Also, NIRF images (IVIS® II Lumina, Caliper LifeSciences, Hopkinton, MA) of the phantom were acquired (excitation: 675 nm, emission: Cy5.5, exposure time: 1 s, binning: small, F/stop: 8, lamp power: high, FOV: D, sample height: 1.98 cm).

2.5. Intracellular uptake of GS nanoparticles

Squamous cell carcinoma (SCC7) cells were provided by Dr. Kwangmeyung Kim (Korea Institute of Science and Technology, KIST, South Korea). SCC7 cells were cultured by using RPMI 1640 (ATCC, Manassas, VA) containing 10% (v/v) FetalPlex™ (Gemini Bioproducts, West Sacramento, CA) at 37 °C in an incubator supplied with 5% CO_2. The cells (about 1×10^5) were incubated in cover glass-bottom dishes (SPL Lifesciences, Pochen, South Korea). When they reached 70–80% confluency, cells were washed twice with phosphate buffered saline (PBS) including calcium and magnesium to eliminate the remnant culture medium and dead cells. The PBS was replaced by the reduced serum medium, Opti-MEM I with Glutamax (Invitrogen, Paisley, UK) and incubated for 30 min. GS nanoparticles (1 mg) were dissolved in Opti-MEM I with Glutamax (1 ml) by sonication. This nanoparticle suspension (50 μl) was mixed with Opti-MEM (950 μl) and seeded in each

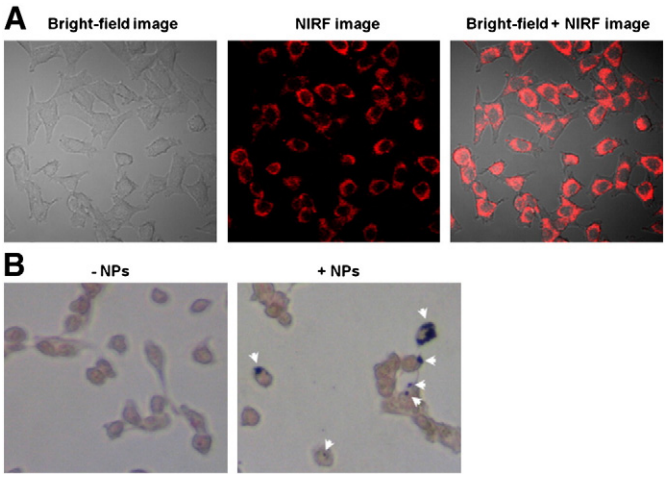

Fig. 4. (A) Intracellular uptake of Cy5.5 dye that was incorporated within GS nanoparticles was demonstrated by using confocal imaging (excitation: 675 nm, emission: 695 nm). (B) Intracellular uptake of SPIOs that were encapsulated in GS nanoparticles was demonstrated by using Prussian blue staining and nuclear fast red counterstaining. White arrows indicate Prussian blue staining by SPIOs in the GS nanoparticles. Prussian blue staining is not very sensitive compared to fluorescent staining and therefore appears more heterogeneous than it really is.

cell culture dish. The cells with the nanoparticles were incubated for up to 4 h at 37 °C. After the incubation, the nanoparticle mixture was removed and the cells were washed with PBS three times. Confocal microscopy images were obtained to confirm intracellular uptake of the GS nanoparticles at 60× magnification using an Olympus IX70 confocal microscope (Center Valley, PA). Excitation (675 nm) and emission (695 nm) were utilized for the NIRF fluorescence of Cy5.5. In order to confirm the intracellular uptake of SPIOs, Prussian blue staining was also performed on these cells with nuclear fast red staining used for counter staining [18]. For that, SCC7 cells were cultured for 24 h in glass-bottom flasks. SCC7 cells were then washed with PBS, resuspended in serum free RPMI 1640 medium, and incubated with GS nanoparticles (200 μg) for 5 h at 37 °C. The medium and remnant GS nanoparticles were washed by washing the SCC7 cells with PBS three times. The cells were fixed with 4% glutaraldehyde solution (1 ml) for 10 min. After washing the solution three times with PBS, the fixed cells were incubated with 2% potassium ferrocyanide in 6% hydrochloric acid for 30 min and counterstained with nuclear fast red. Finally, the intracellular uptake of SPIOs was confirmed using a Nikon Optiphot fluorescence microscope.

2.6. Xenograft studies

C3H/HeN mice (male, 3–4 week old, n = 4, average weight = 20 g) were allowed 7 days of acclimatization and the right flank was shaved 2 days prior to tumor cell implantation. The murine squamous cell carcinoma cells (SCC7) were grown in RPMI 1640 medium, supplemented with 10% fetal bovine serum and l-glutamine at 37 °C and 5% CO_2, and injected intradermally on the flank of each mouse (inoculum size 1×10^6). Mice were anesthetized with isoflurane gas during implantation. GS nanoparticles (5 mg/kg) were injected via tail vein (n = 3) and peritumorally (n = 1) when tumors reached a size of approximately 8–10 mm in diameter 88 h prior to imaging.

2.7. In vivo NIRF imaging

The SCC7 tumor bearing mice were visualized by using the eXplore Optix System (ART Advanced Research Technologies Inc., Montreal, Canada). During imaging, mice were anesthetized with isoflurane gas. A 670 nm pulsed laser diode was used to excite the Cy5.5 molecules within the GS nanoparticles. Emission wavelength at 700 nm was collected and detected with a fast photomultiplier tube (Hamamatsu, Japan) and a time-correlated single-photon counting system (Becker and Hickl GmbH, Berlin, Germany). NIRF images of major organs and tumors were obtained with a 12-bit CCD camera (Kodak Image Station 4000MM, New Haven, CT) and a Cy5.5 bandpass emission filter (680 nm to 720 nm; Omega Optical).

2.8. In vivo MRI

3 T MR images were obtained at 24 h post-injection of GS nanoparticles using the following conditions: T_2-map, axial plane, 2D, TR = 1500 ms, TE = 9, 17, 26, 35, 44, 53, 62, and 72 ms, FOV = 100 mm, 8HRBRAIN coil, Frequency/Phase = 256/256. For in vivo MRI, mice were anesthetized by injecting the mice with a mixture of Ketamine (90 mg/kg) and Xylazine (10 mg/kg) in saline. The final MR images at tumor sites were pseudo-colored using Sante DICOM viewer software (Athens, Greece).

2.9. TEM imaging of excised tumors

After in vivo imaging, tumor-bearing mice were euthanized by intraperitoneal injection of pentobarbital (100 mg/kg). Mice were necropsied to note any gross changes due to administration of nanoparticles and tumors harvested from these mice. Tissue TEM images of their tumors were obtained to confirm the intracellular uptake of GS nanoparticles in SCC7 tumors. To prepare tissues for TEM imaging, the dissected tumor tissues were fixed in 3% glutaraldehyde in 0.1 M cacodylate buffer (pH 7.4) using the microwave method. The fixed tumors were treated with 1% OsO_4 and 1.5% $K_3Fe(CN)_6$. The samples were then dehydrated with graded ethanol series (from 10% to 100%) and propylene oxide. Next, they were embedded in a Petri dish with capsules and polymerized for 48 h at 60 °C. Blocks of the embedded samples were trimmed using razor blades and then cut into thin sections using an ultramicrotome (thickness: 80–100 nm). Finally, the sectioned samples were placed on support grids with a carbon-coated polymer film. TEM images were acquired on an FEI/Philips CM-10 TEM (FEI Company, Hillsboro, OR) using an acceleration voltage of 80 kV and 28.5 K magnification. The TEM images were obtained without additional staining processes since many SCC7 cell organelles looked like SPIOs (black dots) after the staining processes. Finally, the TEM images of tumors from mice

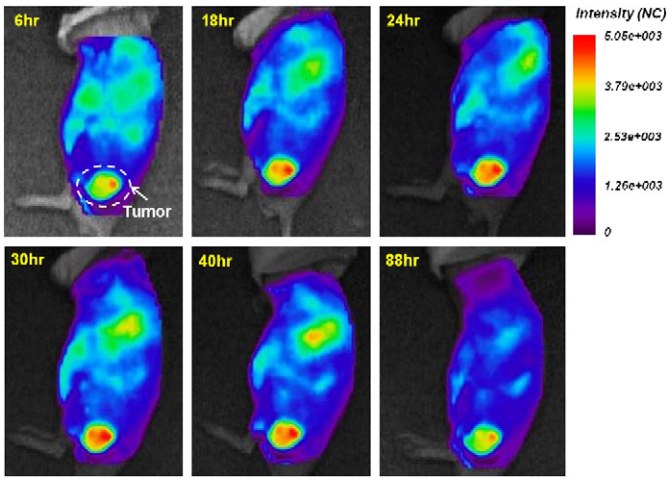

Fig. 5. In vivo NIRF images of GS nanoparticle biodistribution in live mice. GS nanoparticles were injected via tail vein injection. NIRF signals arising from fluorescence of Cy5.5 NIRF dye incorporated into GS nanoparticle constructs were then tracked at various time points ranging from 6 h to 88 h post-injection. Predominant accumulation of GS nanoparticles at the tumor site was observed. All images had normalized NIRF intensities. Tumor is indicated by using a white dashed circle and solid white arrow.

Table 1
Characterization of GS nanoparticles.

Sample	Feed ratio of Fe (wt.%)	Loading efficiency (%)	Average diameter (nm)
GS nanoparticles	6.64	50	349 ± 10

which had received administration of GS nanoparticles via tail vein or peritumorally were compared.

3. Results and discussion

3.1. Physicochemical properties of GS nanoparticles

Glycol chitosan (GC) polymers were chemically conjugated to hydrophobic 5β-cholanic acid molecules and these GC conjugates were labeled with Cy5.5 near-infrared fluorescent (NIRF) dye, resulting in HGC nanoparticles (Fig. 1B). Next, we physically loaded oleic acid capped SPIOs into HGC nanoparticles for in vivo NIRF and MRI dual-modality imaging (Fig. 1A). Oleic acid capped SPIOs were stable in chloroform and maintained a consistent size range for 6 months (data not shown). The mean diameter of oleic acid capped SPIOs was 4 nm in TEM images (Fig. 2A). The hydrophobic oleic acid capped SPIOs were easily incorporated into the hydrophobic 5β-cholanic acid positioned at the inside of the HGC particles. The size and shape of GS nanoparticles were then evaluated by TEM. Since SPIOs and HGC nanoparticles have different extents of X-ray absorption, both HGC and SPIO nanoparticles could be detected in TEM images. SPIOs appeared darker than HGC nanoparticles. Most SPIOs were detected inside HGC nanoparticles. The diameters of GS nanoparticles visualized by TEM were about 250–300 nm (Fig. 2B). We also evaluated the diameters of GS nanoparticles in water using DLS. The average diameter of GC nanoparticles in water was about 350 nm which was greater than the average diameter observed by TEM (Fig. 2C). Since we prepared dried samples for TEM images, the average diameter could be less. Also the average diameter of the GC nanoparticles was measured by DLS over a15 day time period to evaluate GC stability in water (Fig. 2D).

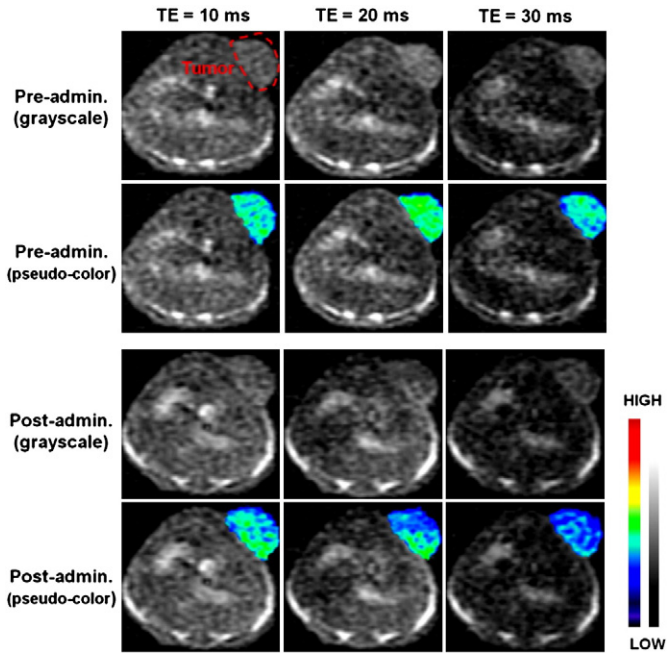

Fig. 6. In vivo MRI was performed by using 3 T MRI and an 8 channel head coil. Various TEs were applied to find enhanced contrast effects by GS nanoparticles. At 20 and 30 ms, we were able to find the T2 effects of GS nanoparticles at the tumor sites. Tumor was indicated by using a white dashed circle.

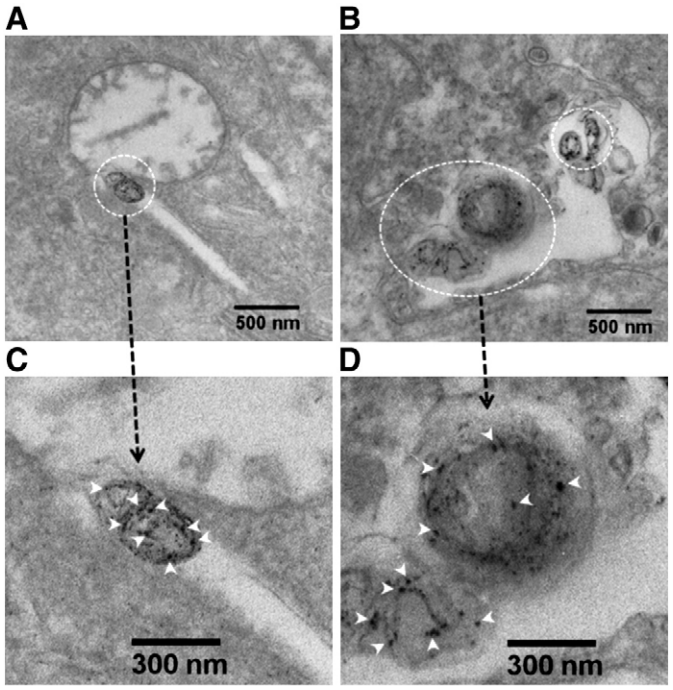

Fig. 7. TEM images showing the intracellular uptake of SPIOs in SCC7 cells. The blocks of tumor were cut into thin sections using an ultramicrotome (thickness: 80–100 nm). Peritumoral injection of GS nanoparticles (A) demonstrated some SPIOs inside the cells. Also, the expanded image (C) showed assembled SPIOs. Tail vein injection of GS nanoparticles (B) also demonstrated individual SPIOs in SCC7 cells. In the expanded image (D), SPIOs were irregularly distributed in the cells. Dashed, white circles indicate the regions featured in the expanded images. Dashed, black lines and black arrows indicate the expanded region to which each circled area corresponds. White arrow heads indicate SPIOs.

When we loaded SPIOs into the HGC nanoparticles, the feed ratio of Fe ions was 6.64 wt.% and the loading efficiency of Fe amount in GS nanoparticles was 50%, which was calculated from the result of ICP-MS (Supplementary data). The average hydrodynamic diameter of GS nanoparticles was 349 ± 10 which was measured by DLS (Table 1).

The r^2 value of the GS NPs was calculated by the formula, $Ri = 1/Ti = (1/Ti)_0 + riC$ where Ri is the relaxation rate of the aqueous solution, Ti_0 is the relaxation time of water without contrast agents, C is the concentration of the contrast agent (mM), ri is relaxivity (S^{-1} mM^{-1}). $T2$ of GS NPs was 44.6 ms and $T2_0$ of water was 2700 ms. C was 0.08 mM. In result, GS NPs showed 280 S^{-1} mM^{-1} which was approximately 2.33 times better than Feridex® approved by FDA for the detection of liver lesions [19]. Other characterizations of GS NPs including chemical conjugation parts and NIRF quantum yield of HGC NPs were shown by our previous research [8,20]. We followed previously published protocols to synthesize HGC NPs and to label NIRF dyes with them.

3.2. Visualization of GS nanoparticles in MR and NIRF imaging

We evaluated the effects of GS nanoparticles as an MR contrast agent and a NIRF imaging probe. T2 effect of GS nanoparticles in water was tested by using 3 T MRI. We compared HGC nanoparticles with GS nanoparticles. The nanoparticles (1 mg/ml) were prepared in nanowater and added into the tissue culture well-plates with successive half-dilutions. At the shortest echo time studied, we could not observe substantial T2 effects in both HGC and GS nanoparticles. However, at the longer echo times, the higher T2 effect from GS nanoparticles was observed. As a result, the GS nanoparticles worked well in T2 weighted MR images. Also, we evaluated the origin of the T2 effect in GS nanoparticles. We concluded the T2 effects came from the loaded SPIOs while HGC nanoparticles barely represented the T2 effects (Fig. 3A). Next, we tested GS nanoparticles in tissue phantom models. Phantom tests were also

important because T2 effects by GS nanoparticles could be changed by different circumstances such as water, lipid, and tumor at which hydrogen protons are in different chemical structures and distribution. Therefore, we prepared the phantom model to mimic tumors and evaluated the T2 effect with 3 T MRI and NIRF intensity with IVIS II Lumina. In both MRI and NIRF imaging, GS nanoparticles functioned both to darken the signal as a negative MRI contrast agent in a T2 weighted image (Fig. 3B) and to brighten the signal in NIRF imaging (Fig. 3C).

3.3. Intracellular uptake of GS nanoparticles

Intracellular uptake of the SPIO-loaded HGC composite GS nanoparticles was evaluated in SCC7 cells. The loaded SPIOs in HGC nanoparticles did not highly affect the intracellular uptake of GS nanoparticles in SCC7 cells. The GS NPs were stable in the serum containing cell culture medium at 37 °C in an incubator supplied with 5% CO_2, not showing precipitation of either HGC NPs or SPIOs. The high intracellular uptake observed in this study might be explained by the protonated properties of chitosan. The primary amine groups on chitosan are protonated in acidic solutions below pH 6.5 [21]. The protonated feature of an acidic solution might increase the affinity of the GS nanoparticles on the cell membranes at the acidic conditions. Under in vivo systems, it might be also possible that the unionized amines on the chitosan nanoparticles at pH 7.4 can maintain a long circulation time in blood and the protonated amines on the nanoparticles at the slightly acidic tumor extracellular matrix can facilitate the intracellular uptake of the nanoparticles. Herein, confocal microscopy images of the Cy5.5 NIRF fluorescence that show the sub-cellular localization of GS nanoparticles were overlaid with bright field images acquired of the same cells. Clear NIRF intensities were observed within the cytoplasm of the SCC7 cells (Fig. 4A). We also confirmed the result by comparing it with the result of Prussian blue staining. Cells were counterstained by fast nuclear red staining (Fig. 4B).

3.4. In vivo NIRF imaging

We evaluated the capability of GS nanoparticles as a contrast agent for NIRF imaging to visualize tumors. NIRF images of biodistribution of GS nanoparticles in live mice were acquired at different time points. At 6 h post-injection of GS nanoparticles, strong NIRF signals were distributed throughout the body although the NIRF signals at the tumor site were slightly stronger than at other parts. At 24, 30, and 40 h post-injection, a consistent increase in the NIRF signals at the tumor site was observed while the signals from the other parts of the body gradually decreased with time, with the exception of the liver. However, the signal at tumor remained approximately 1.3 times stronger than the signals observed at the liver. At 88 h, all the NIRF signals were decreased, but the intensity at the tumor site was still stronger than the other parts (Fig. 5). This result suggested that GS nanoparticles circulated throughout the body and were excreted within 3 days time. Most NIRF signals from GS nanoparticles disappeared over time except for the signals at the tumor site. This effect can be explained by EPR effect [4,22]. Angiogenesis is the process of development of blood vessels around tumor sites to persistently supply oxygen and nutrients to the tumors. Due to the rapid growth of the blood vessels, wider interstitial gaps between endothelial cells are formed than are normally found in blood vessels, resulting in the enhanced permeability of these vessels to foreign substances such as nanoparticles (generally 10 to 500 nm) than occurs with normal blood vessels. Also, because of the lack of lymphatic drainage in the rapidly growing blood vessels, the substances can be retained for a longer time than usual [23]. However, we noticed that the enhanced retention effect is limited. The NIRF signals observed at the tumor site were also decreased after 88 h.

3.5. In vivo MRI

In vivo MRI was performed by using 3 T MRI. We utilized T2-weighted sequences with different echo times using an 8 channel head coil. When the echo time is short, it is hard to observe any T2 contrast effect because many protons in the body precess in a phase. On the other hand, when the echo time is very long, every signal including signals from the body itself will disappear due to the dephasing effects of protons. We did not observe significant differences between pre-administration and post-administration of GS nanoparticles at the shortest echo time studied (10 ms). However, T2 contrast effects at tumor sites were observed in the post-administration of GS nanoparticles at the longer echo times (20 ms and 30 ms). We also converted the grayscale MR images to pseudo-colored images. The tumor region of post-administration of GS nanoparticles was in the blue range of the MR image spectrum while the tumor region of pre-administration of the nanoparticles was in the green range (Fig. 6). This result also suggests that even better sensitive imaging could be achieved by either smaller coil or higher Tesla MRI.

3.6. TEM images of excised tumor tissues

The intracellular positions of GS nanoparticles in mice were further investigated in excised tumor tissues by TEM imaging. GS nanoparticles were administered in tumor bearing mice via tail vein ($n=3$) and peritumorally ($n=1$). At 24 h post-injection, mice were sacrificed and tumors were excised and fixed. Additional staining processes were not necessary because the electron dense of SPIOs was detected as dark black spots in TEM images. In the TEM images, some SPIOs were found in both cases. However, the original spherical shape of GS nanoparticles was rarely observed. GS nanoparticles can be dissociated in acidic condition such as endosomes or lysosomes. At acidic conditions below pH 6.5, the primary amine groups on chitosan are protonated [21], which might accelerate the dissociation of SPIOs from the carrier (Fig. 7).

4. Conclusion

In our previous study, optical imaging indicated that HGC nanoparticles demonstrated highly selective accumulation at tumor sites. In this study, we tried to expand the functionality of these nanoparticles for MRI. The utility of adding MRI imaging capability to our HGC nanoparticles is the incorporation of a second imaging modality. The enhanced image quality provided by MR contrast agents will provide more opportunities for early-stage cancer detection even at locations deep within the human body that cannot be seen by fluorescence under normal conditions due to loss of signal with tissue depth. However, while beyond the scope of this paper, the fluorescence in-vivo measurements start to become important during real-time fluorescent-guided surgery whereby the margins of the tumor can be seen with high accuracy, representing a potentially major advance to surgeons who can now see more accurately the true margins of the tumors. In addition, nanoparticles such as GS nanoparticles can be used for optical imaging, in this case for NIRF-image guided surgery. In this study we demonstrated, using both in vitro and in vivo experiments, the possibility of using GS nanoparticles as NIRF and MR dual-modality imaging agents. However, depending on the tumor size, the targeting capability of GS NPs might be changed due to differing angiogenesis surrounding the tumor as well as effects of necrosis as the tumor grows larger. For future works, we will also compare different aspects of tumor accumulation of GS NPs with respect to different tumor sizes. Nevertheless, this result still emphasizes the possibility of early detection of cancer using optical and MRI with GS NPs. For future studies, we will also evaluate active targeting nanoparticles using tumor specific ligands in combination with anti-cancer drugs.

Acknowledgments

This work was supported by KIST-Purdue GRL (Global Research Laboratory) Collaboration, "Molecular Imaging and Nanomedicine for Theragnosis using NanoBioMaterials"; Grant number: 202979 and the Christopher Columbus Foundation support to JFL. We would like to especially thank Patty I. Bonney, Lindsey M. Fourez, Jane C. Stewart, and Carol Ann Dowell at Purdue University for their assistance with this work. We also express our appreciation to Dr. Aaron Taylor of the Bindley Bioscience Imaging Facility, Dr. Tom Talavage and Greg Tamer of the Purdue MRI facility at Purdue Research Park, and to Debby Sherman and Chia-Ping Huang of the Life Sciences Microscopy Facility at Purdue University for the TEM images, and to Lisa Reece of the Bionano Facility in the Birck Nanotechnology Center supported in part by the Indiana Clinical and Translational Sciences Institute from the National Institutes of Health, National Center for Research Resources, Clinical and Translational Sciences Award.

Appendix A. Supplementary data

Supplementary data to this article can be found online at http://dx.doi.org/10.1016/j.jconrel.2012.07.038.

References

[1] H. Varmus, The new era in cancer research, Science 312 (2006) 1162–1165.
[2] M.A. Davis, S. Hanash, Plasma-based proteomics in early detection and therapy, Breast Cancer Res. 8 (2006) 217.
[3] R. Etzioni, N. Urban, S. Ramsey, M. McIntosh, S. Schwartz, B. Reid, J. Radich, G. Anderson, L. Hartwell, The case for early detection, Nat. Rev. Cancer 3 (2003) 243–252.
[4] H. Maeda, Tumor-selective delivery of macromolecular drugs via the EPR effect: background and future prospects, Bioconjug. Chem. 21 (2010) 797–802.
[5] V. Ntziachristos, C. Bremer, R. Weissleder, Fluorescence imaging with near-infrared light: new technological advances that enable in vivo molecular imaging, Eur. Radiol. 13 (2003) 195–208.
[6] J. Cheon, J.H. Lee, Synergistically integrated nanoparticles as multimodal probes for nanobiotechnology, Acc. Chem. Res. 41 (2008) 1630–1640.
[7] K. Kim, J.H. Kim, H. Park, Y.S. Kim, K. Park, H. Nam, S. Lee, J.H. Park, R.W. Park, I.S. Kim, K. Choi, S.Y. Kim, K. Park, I.C. Kwon, Tumor-homing multifunctional nanoparticles for cancer theragnosis: simultaneous diagnosis, drug delivery, and therapeutic monitoring, J. Control. Release 146 (2010) 219–227.
[8] K. Park, J.H. Kim, Y.S. Nam, S. Lee, H.Y. Nam, K. Kim, J.H. Park, I.S. Kim, K. Choi, S.Y. Kim, I.C. Kwon, Effect of polymer molecular weight on the tumor targeting characteristics of self-assembled glycol chitosan nanoparticles, J. Control. Release 122 (2007) 305–314.
[9] R. Weissleder, M.J. Pittet, Imaging in the era of molecular oncology, Nature 452 (2008) 580–589.
[10] T. Nam, S. Park, S.-Y. Lee, K. Park, K. Choi, I.C. Song, M.H. Han, J.J. Leary, S.A. Yuk, I.C. Kwon, K. Kim, S.Y. Jeong, Tumor targeting chitosan nanoparticles for dual-modality optical/MR cancer imaging, Bioconjug. Chem. 21 (2010) 578–582.
[11] H.H. Abujudeh, R. Kaewlai, A. Kagan, L.B. Chibnik, R.M. Nazarian, W.A. High, J. Kay, Nephrogenic systemic fibrosis after gadopentetate dimeglumine exposure: case series of 36 patients, Radiology 253 (2009) 81–89.
[12] Z. Ali, A.Z. Abbasi, F. Zhang, P. Arosio, A. Lascialfari, M.F. Casula, A. Wenk, W. Kreyling, R. Plapper, M. Seidel, R. Niessner, J. Knöll, A. Seubert, W.J. Parak, Multifunctional nanoparticles for dual imaging, Anal. Chem. 83 (2011) 2877–2882.
[13] Y. Yu, D. Sun, Superparamagnetic iron oxide nanoparticle theranostics for multimodality tumor imaging, gene delivery, targeted drug and prodrug delivery, Expert. Rev. Clin. Pharmacol. 3 (2010) 117–130.
[14] J.H. Na, H. Koo, S. Lee, K.H. Min, K. Park, H. Yoo, S.H. Lee, J.H. Park, I.C. Kwon, S.Y. Jeong, K. Kim, Real-time and non-invasive optical imaging of tumor-targeting glycol chitosan nanoparticles in various tumor models, Biomaterials 32 (2011) 5252–5261.
[15] J. Park, G. Saravanakumar, K. Kim, I. Kwon, Targeted delivery of low molecular drugs using chitosan and its derivatives, Adv. Drug Deliv. Rev. 62 (2010) 28–41.
[16] U.I. Tromsdorf, N.C. Bigall, M.G. Kaul, O.T. Bruns, M.S. Nikolic, B. Mollwitz, R.A. Sperling, R. Reimer, H. Hohenberg, W.J. Parak, Size and surface effects on the MRI relaxivity of manganese ferrite nanoparticle contrast agents, Nano Lett. 7 (2007) 2422–2427.
[17] W.W. Yu, J.C. Falkner, C.T. Yavuz, V.L. Colvin, Synthesis of monodisperse iron oxide nanocrystals by thermal decomposition of iron carboxylate salts, Chem. Commun. 2004 (2004) 2306–2307.
[18] D. Kim, N. Lee, M. Park, B.H. Kim, K. An, T. Hyeon, Synthesis of uniform ferrimagnetic magnetite nanocubes, J. Am. Chem. Soc. 131 (2009) 454–455.
[19] N. Lee, T. Hyeon, Designed synthesis of uniformly sized iron oxide nanoparticles for efficient magnetic resonance imaging contrast agents, Chem. Soc. Rev. 41 (2012) 2575–2589.
[20] S. Kwon, J. Park, H. Chung, I. Kwon, S. Jeong, Physicochemical characteristics of self-assembled nanoparticles based on glycol chitosan bearing 5-cholanic acid, Langmuir 19 (2003) 10188–10193.
[21] W. Liu, S. Sun, Z. Cao, X. Zhang, K. Yao, W.W. Lu, K.D.K. Luk, An investigation on the physicochemical properties of chitosan/DNA polyelectrolyte complexes, Biomaterials 26 (2005) 2705–2711.
[22] Y. Matsumura, H. Maeda, A new concept for macromolecular therapeutics in cancer chemotherapy: mechanism of tumoritropic accumulation of proteins and the antitumor agent Smancs, Cancer Res. 46 (1986) 6387–6392.
[23] V. Torchilin, Tumor delivery of macromolecular drugs based on the EPR effect, Adv. Drug Deliv. Rev. 63 (2011) 131–135.